Solid Earth Discuss., 5, 1901–1940, 2013
www.solid-earth-discuss.net/5/1901/2013/
doi:10.5194/sed-5-1901-2013

Solid Earth
Discussions
Open Access

Focal mechanism and depth of the 1956 Amorgos twin earthquakes from waveform matching of analogue seismograms

A. Brüstle[1], W. Friederich[1], T. Meier[2], and C. Gross[3]

[1]Institute of Geology, Mineralogy and Geophysics, Ruhr-University Bochum, Germany
[2]Institute of Geosciences, Christian-Albrechts-University, Kiel, Germany
[3]formerly at Institute of Geology, Mineralogy and Geophysics, Ruhr-University Bochum, Germany

Received: 2 September 2013 – Accepted: 26 October 2013 – Published: 11 November 2013

Correspondence to: A. Brüstle (andrea.bruestle@ruhr-uni-bochum.de)

Published by Copernicus Publications on behalf of the European Geosciences Union.

Abstract

Historic analogue seismograms of the large 1956 Amorgos twin earthquakes which occurred in the volcanic arc of the Hellenic Subduction Zone (HSZ) were collected, digitized and reanalyzed to obtain refined estimates of their depth and focal mechanism. In total, 80 records of the events from 29 European stations were collected and, if possible, digitized. In addition, bulletins were searched for instrument parameters required to calculate transfer functions for instrument correction. A grid search based on matching the digitized historic waveforms to complete synthetic seismograms was then carried out to infer optimal estimates for depth and focal mechanism. Owing to incomplete or unreliable information on instrument parameters and frequently occurring technical problems during recording such as writing needles jumping off mechanical recording systems, much less seismograms than collected proved suitable for waveform matching. For the first earthquake, only 7 seismograms from three different stations (STU, GTT, COP) could be used. Nevertheless, the grid search produces stable optimal values for both source depth and focal mechanism. Our results indicate a shallow hypocenter at about 25 km depth. The best-fitting focal mechanism is a SW–NE-trending normal fault dipping either by 30° towards SE or 60° towards NW. This finding is consistent with the local structure of the Santorini–Amorgos graben. For the second earthquake, 4 seismograms from three different stations (JEN, GTT, COP) proved suitable for waveform matching. Whereas it was impossible to obtain meaningful results for the focal mechanism owing to surface wave coda of the first event overlapping body wave phases of the second event, waveform matching and time-frequency analysis point to a considerably deeper hypocenter located within the Wadati–Benioff-zone of the subducting African plate at about 120–160 km depth.

1 Introduction

On 9 July 1956 (03:11 GMT), one of the strongest earthquakes of the 20th century in the southern Aegean occurred between the islands of Amorgos and Santorini with a magnitude of $M_S = 7.4$ (Makropoulos et al., 1989). A second strong earthquake (03:24 GMT) with a magnitude of $M_S = 7.2$ occurred just 13 min later in the same region. Both earthquakes were located in the Santorini–Amorgos graben within the central volcanic arc (HVA) of the Hellenic Subduction Zone (HSZ, Fig. 1). The first earthquake was located at the northern flank of the graben southwest of Amorgos (Comninakis and Papazachos, 1986; Makropoulos et al., 1989; Okal et al., 2009). Epicenter locations of the second earthquake vary from the northern graben shoulder southwest of Amorgos (Comninakis and Papazachos, 1986) and the northeastern Santorini–Coloumbo volcanic complex (Makropoulos et al., 1989) to the southern graben shoulder near Anafi (Okal et al., 2009).

The HSZ is the seismically most active region of the Europe-Mediterranean region (McKenzie, 1972; Papazachos, 1977). Here, the oceanic African slab segment, the Hellenic slab, is subducting to the north beneath the continental Aegean plate with a relative velocity of 4 cm yr^{-1} (McKenzie, 1970; Reilinger et al., 2006). Due to the rollback of the Hellenic slab the Aegean plate is under extensional strain leading to a thinning of the crust (25–27 km) beneath the southern Aegean as evidenced from seismic reflection profiles (Makris, 1978; Bohnhoff et al., 2001), receiver function analysis (Sodoudi et al., 2006, 2013), gravity analysis (Tirel et al., 2004) and tomographic studies (Drakatos et al., 1997; Papazachos and Nolet, 1997; Karagianni et al., 2002, 2005; Karagianni and Papazachos, 2007; Endrun et al., 2008). Shallow seismicity of the central HVA is dominantly located within the upper crust of the Aegean plate at hypocenter depths of less than 15–20 km and follows the northern Santorini–Amorgos graben shoulder southwest of Amorgos. The northern graben southeast of Amorgos only shows low seismic activity (Bohnhoff et al., 2006; Brüstle, 2012). Stress tensor inversions of fault plane solutions (Bohnhoff et al., 2006; Friederich et al., 2013) lived from available first P motion polarities of shallow high-quality hypocenter locations indicate a SE–NW oriented tensional principal stress axis. The Santorini–Coloumbo volcanic complex is located in the southern extension of the western Santorini–Amorgos graben shoulder. During the last 60 yr the Santorini volcano exhibited only weak background seismicity (Dimitriadis et al., 2005; Bohnhoff et al., 2006; Dimitriadis et al., 2009; Hensch, 2009), except for a period of unusual high seismicity lasting from January 2011 to January 2012 with local magnitudes up to 3.2 accompanied by surface deformations within the Caldera as a result of magma upwelling (Newman et al., 2012; Chouliaras et al., 2012; Vallianatos et al., 2013). In contrast, the submarine Coloumbo volcano is characterized by continuous high seismic activity and volcanic unrest. Local seismicity occurs at depths of 3–9 km within a 3 km wide vertical column beneath the northeastern flank of the submarine volcano as a result of magmatic intrusions (Dimitriadis et al., 2005; Bohnhoff et al., 2006; Kolaitis et al., 2007; Dimitriadis et al., 2009; Hensch, 2009). Focal mechanisms of these earthquakes also show preferably NE–SW striking normal faulting mechanisms implying a strong connection to the Kameni-Coloumbo fracture, the southern extension of the western Santorini–Amorgos fault zone. Intermediate-depth seismicity is observed at 120–160 km depth indicating the Wadati–Benioff Zone (WBZ) of the subducting Hellenic slab (Knapmeyer, 1999; Papazachos et al., 2000; Meier et al., 2007; Brüstle, 2012).

The island Amorgos is part of the northern footwall of the graben structure. Neotectonic investigations on Amorgos infer a tensional NW–SE trending stress pattern (Papadopoulos and Pavlides, 1992) and backtilting (subsidence of the north coast, uplift of the south coast) of the island (Stiros et al., 1994). The southern coastline of the island has been uplifted by about 30 cm as a result of the seismic activity in July 1956. Seismic reflection profiles of the Santorini–Amorgos graben point to a large recent sediment slumping event between Santorini and Amorgos, which is also associated to the seismic activity in July 1956 (Perissoratis and Papadopoulos, 1999).

The shallow origin of at least one of the earthquakes seems to be evident from the reported tsunami waves, which caused damages within a region of about 100 km (Ambraseys, 1960; Stiros et al., 1994). Detailed studies were undertaken to determine wave heights and wave runups on the islands in the southern Aegean. Highest sea wave amplitudes (Fig. 1) were observed at the south coast of Amorgos (20–30 m) and the north coast of Astypalea (10 m) by eye witnesses as well as marine flood deposits (Ambraseys, 1960; Galanopoulos, 1960; Dominey-Howes, 1996; Dominey-Howes et al., 2000; Okal et al., 2009), whereas at the coastlines of the two islands averted from the Santorini–Amorgos graben structure as well as at the northern coastline of Crete, on the Dodecanese islands and the Turkish W-coast wave amplitudes of less than 4 m were observed. The only exception is the island Folegandros, where locally wave amplitudes of up to 14.6 m were observed at the western coast.

Both earthquakes caused severe damages on the surrounding islands, especially on Santorini and Astypalea. In total, 53 people were killed, 100 people were injured, 529 buildings were destroyed. More than 3200 buildings were severely damaged. Most of them were reported on Santorini, where the second event apparently effected the final collapse of houses already damaged by the first event (Ambraseys, 1960; Galanopoulos, 1982).

While the two earthquakes have been unanimously located in the Santorini–Amorgos graben, focal parameters and focal depth are controversial (Tab. 1), or affected by large uncertainties (Galanopoulos, 1982; Comninakis and Papazachos, 1986; Makropoulos et al., 1989). For the first event, (Shirokova, 1972) proposed a fault plane solution of a ENE–WSW striking normal fault with a slight dip to SSE calculated from first-motion polarities of *P* phases (Fig. 2), which has been confirmed by stress pattern determination from field observations. Other fault plane solutions indicating a strike-slip solution (Papazachos and Delibasis, 1969; Ritsema, 1974) were judged of poor quality by the authors themselves. The focal mechanism of the second event is essentially unknown.

Since the data were recorded on analogue devices and mostly written on paper, the only way to reassess these important earthquakes using modern seismological techniques is by collecting, digitizing and reprocessing historic analogue recordings. Re-

SED
5, 1901–1940, 2013

cently, (Okal et al., 2009) digitized teleseismic recordings of the first event and inverted them for the spectral amplitudes of mantle Rayleigh and Love waves and obtained a SW–NE striking normal faulting at focal depth of about 45 km. In the study reported here, analogue seismograms and bulletins of regional stations were collected to refine estimates of focal parameters and focal depth of the two earthquakes. The scanned analogue seismograms were digitized and analyzed for their frequency content using a multiple filter technique after (Dziewonski et al., 1969). The MFT allowed to identify P, S and surface waves of the first event and to distinguish body waves of the second earthquake from surface wave coda of the preceding one. Finally, a grid-search was applied based on cross-correlation and waveform matching of the digitized analogue seismograms with synthetic waveforms to determine the best fitting focal mechanism and hypocenter depth of the two earthquakes. Unfortunately, waveform matching proved impossible for the second event because of severe overlap of the surface wave coda of the first event with the body wave phases of the second event at regional distances.

2 Analogue seismograms and instrument parameters

Based on the International Seismological Summary (ISS) of 1956 the two major Amorgos earthquakes were recorded at 317 (first event) respectively 60 (second event) stations world-wide. In total, more than 80 analogue seismograms from 29 European stations were collected (Fig. 3) to reinvestigate the first and, if possible, the second earthquake of 9 July 1956. Seismograms were collected by the first author and mostly scanned within the SISMOgrammi Storici SISMOS project (Michelini et al., 2005) or obtained already scanned from the SISMOS database. The collection of analogue seismograms covers dominantly western and northwestern Europe with an azimuthal coverage of 120° and regional distances of 247 to 2337 km. The digitization of the seismograms was done with a plug-in for the GNU Image Manipulation Program GIMP called TESEO (Pintore et al., 2005). The software allows to apply geometrical corrections of the digitized seismogram (e.g. curvature of the writing arm, skewness of the recording) and to resample the digitized waveform to equally spaced data points.

In addition, bulletins and reports were searched or taken from the SISMOS database to gain detailed information on instrument dimensions and parameters for further processing. This is very important, as seismometer instruments were not standardized at that time. Most observatories had their unique seismograph with individual orientation of the instrument and polarization of the components. To obtain sufficient amplification, the damping of the instruments was either very weak in comparison to today or instruments were recording without any damping (e.g. vertical pendulum at Ebro EBR in Spain, Milne-seismograph at Malta, MLT). Also, each observatory was adjusting instrument parameters quite frequently to obtain the best resolution on the recording paper. Figure 4 (left) shows e.g. that at station POT of the Potsdam observatory instrument parameters were adjusted twice in 1957. Unfortunately these adjustments were rarely reported in the bulletins.

At that time, the stations were equipped with mechanical as well as electro-dynamic or electro-magnetic instruments. The recordings were carried out mechanically or galvanometrically on smoked or photographic paper. Because of the absence of broadband seismometers many observatories were equipped with more than one seismograph, each covering a different frequency band. A very impressing example was the station STU at the Stuttgart observatory (Fig. 4, right). During the studied time period about 7 seismograph systems were recording simultaneously.

Due to the large magnitude of the first earthquake, high amplitudes, especially of the surface waves, caused clipping of the waveforms or recording needles jumping off the mechanical recording systems, making a considerable number of recordings unusable for further investigations. Moreover, waveforms are often disturbed by time marks, variable paper speed or, in many cases of photo-optical paper recordings, by insufficient exposure-time. Finally, missing information on instrument parameters (to calculate the instrument response), on orientation and polarization of the components, or just missing station and instrument name annotations on the seismogram paper

SED
5, 1901–1940, 2013

are reasons why even good recordings proved unusable. Figure 5 shows a typical recording of the two earthquakes on the vertical component of the 1300 kg-Wiechert seismograph at the station of Göttingen (GTT, Germany). Body waves (*P*1, *S*1) and surface waves (sf1) of the first event are clearly visible, while the corresponding phases (*P*2, *S*2, sf2) of the second event are overlain by the surface waves coda of the first event.

For both earthquakes only recordings of the fully mechanical systems of Wiechert- or Mainka-seismographs at regional distances of about 17° to 21° (Tab. 2) proved suitable for further investigations. Instrument responses were notated on the seismogram paper or documented in the available bulletins (Tab. 3). The component polarity of station GTT (marked on the seismogram recording) and COP (Copenhagen, Denmark; Charlier and Van Gils, 1953) was inverse, while the component polarity of station STU (R. Schick, personal communication, 2006) and Jena (JEN, Germany; Charlier and Van Gils, 1953) can be assumed to be correct. Figure 6 shows the digitized waveforms sections (black) for the two earthquakes which were suitable for waveform matching. For the first earthquake, they comprise the following phases: *P* and *S* phases on all three components of station GTT, on the *N* component of station COP and *E* component of station STU; the *P* phase only on the *E* component of station COP and the *N* component of station STU. For the second earthquake, three of the four digitized waveforms (GTT-Z, GTT-E, JEN-Z) cover the entire time window of body- and surface waves, whereas only body waves are available on the *N* component of station COP.

3 Instrument responses

In a first step transfer functions were calculated from available instrument parameters. The standard transfer function of a fully mechanical seismograph-system is defined by

SED
5, 1901–1940, 2013

the following expression:

$$|H(\omega)| = A \frac{\omega^2}{\sqrt{(\omega_0^2 - \omega^2)^2 + 4d_s^2\omega_0^2\omega^2}}, \qquad (1)$$

where d_s is the damping constant, ω_0 is the angular eigenfrequency of the instrument and A a frequency-independent calibration factor (Schick and Schneider, 1973). In general, the instrument parameters eigenperiod (T_0), damping ratio (ϵ) and calibration factor (A) are reported in the annual bulletins of the observatories. The damping constant is related to the damping ratio as follows (Galizin, 1914):

$$d_s = \left(\pi^2 + \ln^2\epsilon\right)^{-\frac{1}{2}} \ln\epsilon\,. \qquad (2)$$

Figure 7 shows the frequency-dependent normalized transfer functions of two mechanical seismometers. The transfer function of the Z component of the 1300 kg-Wiechert seismograph at the station GTT shows a nearly optimal damping and a flat response for frequencies above 0.2 Hz and thus ensures a constant amplification of the recorded frequencies. But not all instruments were optimally damped back then. An example is the vertical pendulum at the station EBR, which was completely undamped with a resonance at 0.4 Hz.

4 Multiple filter analysis of the analogue seismograms

To identify different phases in the digitized seismograms and also distinguish phase arrivals of the second event from surface wave coda of the first event, we calculated time-frequency spectra with a multiple filter technique (MFT, Dziewonski et al., 1969). The digitized data are Fast Fourier transformed (FFT) into the frequency domain and fil-

SED
5, 1901–1940, 2013

tered at a series of equidistant center frequencies using narrow Gaussian bandpasses

$$B(\omega,\omega_n) = \begin{cases} \exp\left[-\alpha\left(\frac{\omega-\omega_n}{\omega_n}\right)^2\right] & \text{if } \omega_{l,n} \leq \omega \leq \omega_{u,n} \\ 0 & \text{otherwise}, \end{cases} \quad (3)$$

where ω_n is the center frequency of the filter, $\omega_{l,n}$ and $\omega_{u,n}$ are lower and upper bandpass limits and α controls the resolution of the filter. Note, that α is linearly dependent on frequency in order to optimize the time-frequency resolution (Meier et al., 2004). After inverse FFT, the envelope of the filtered waveform is calculated and displayed as a color-coded function of time with the maximum of the envelope normalized to one. High amplitudes of the envelope are indicated by regions of reddish colors whereas blue colors signify low amplitudes. The time-frequency spectrum of the unfiltered Z component of the 1300 kg-Wiechert seismograph at station GTT (Fig. 8a) clearly shows the non-dispersed P and S phases at 4.5 min and 8 min and the dispersion curve of the surface waves at 8–17 min after event time of the first earthquake. The offset of the dispersion curve at frequencies less than 0.02 Hz corresponds to a vertical displacement (clipped recording) of the recorded seismogram at about 12 min. Phase arrivals of the second event are masked in the seismogram by the coda of the surface waves of the first event. However, the time-frequency-spectra allow to identify the signals of P and S phases at 16.5 and 20 min, while surface waves can not be recognized. The second example shows the unfiltered waveforms of the first and second earthquake recorded by an undamped vertical pendulum at station EBR (Fig. 8b). The amplitude spectrum of this record shows high amplitudes in the range of 0.35–0.45 Hz corresponding to the resonance frequency of the calculated transfer function. Although the undamped signal of EBR is not as clear as the one recorded at station GTT, P (5–7 min) and S (8–10 min) phases as well as the dispersion curve (8–16 min) of the surface waves can be identified for the first earthquake. Though the second earthquake exhibits a weaker signal, P (17–19 min) and S (20–22 min) phases can still be identified. However, as for GTT surface waves are missing, indicating a hypocenter at greater depths probably located in the subducting Hellenic slab.

5 Focal mechanism and hypocenter depth determination from waveform matching

A grid search based on a waveform matching procedure was attempted to obtain best-fitting estimates of the focal mechanism and hypocentral depth. The basic idea is to sweep through all possible hypocentral depths and focal mechanisms characterized by the strike and dip of the fault plane and the slip direction on the fault plane, to determine the corresponding moment tensor with unit seismic moment and to calculate synthetic seismograms for this moment tensor and depth. After scaling the observed waveforms to the maximum rms-value of all data traces and the synthetic waveforms to the rms-value of the corresponding synthetic trace, a misfit over all traces is calculated whose minimum points to the optimal selection of source depth and focal mechanism. Epicentral coordinates, origin time and earth model are kept fixed during the search.

The synthetic seismograms were calculated for the standard 1-D-earth model AK135 (Kennett et al., 1995) using the GEMINI code (Friederich and Dalkolmo, 1995). The program provides complete seismograms for moment tensor point sources in a spherically symmetric earth model. The source time function is a delta function leading to velocity seismograms for a step function moment tensor source. The synthetics were then filtered in the same way as the data and convolved with the instrument response of the corresponding seismograph calculated from the parameters listed in Table 3. Finally, they were cut to the same time window as the corresponding data traces and interpolated to identical sampling times. Further processing encompassed the removal of the average and a possible linear trend due to a drift of the instrument as well as bandpass filtering. Since the synthetics are calculated as velocity waveforms, the data were differentiated in case they were recorded as displacements.

SED
5, 1901–1940, 2013

A direct matching of the instrument corrected synthetics with the digitized data turned out to be unsuccessful because of phase mismatches due to either timing errors in the data or deviations of the true earth structure from the standard earth model used. Timing errors are likely for recordings of the 1950's, where in general time was manually noted on the seismogram paper from a pendulum clock and time adjustments of the pendulum clock were applied from the telephone or radio time signal once a day (Wielandt, 1996). To compensate for these phase mismatches, we first calculate a normalized cross-correlation function of the processed data and synthetics for lag times ranging from −60 s to +60 s,

$$C(\tau) = \frac{\int_0^T s(t+\tau)d(t)\,\mathrm{d}t}{\sqrt{\int_0^T s(t)^2\,\mathrm{d}t}\,\sqrt{\int_0^T d(t)^2\,\mathrm{d}t}}. \tag{4}$$

Then, we identify the time lag associated with the local maximum of the cross-correlation closest to zero lag and time shift the synthetics by this amount. To accommodate amplitude differences between data and synthetics, the data are scaled to the maximum rms-value of all data traces ($d_{\max}$) and the synthetics to the rms-value of the corresponding synthetic trace ($s_{\max}$). Only after these steps, a misfit between data and synthetic trace is calculated as follows:

$$\chi_k^2 = \frac{1}{C_{\max}^2\,T}\int_0^T \left(\frac{s_k(t+\tau)}{s_{\max}} - \frac{d_k(t)}{d_{\max}}\right)^2 \mathrm{d}t. \tag{5}$$

where X_k is the misfit for the $k-th$ trace, $s_k(t)$ is the $k-th$ synthetic trace and $d_k(t)$ the $k-th$ data trace. The scaling is trace-independent and therefore preserves relative amplitude differences between stations and components. The total misfit is evaluated as the sum of the individual trace misfits. The additional weighting of the trace misfits by the inverse maximum cross correlation drives the grid search to solutions associated with a high similarity of data and synthetic traces. Once a best fitting focal mechanism

SED
5, 1901–1940, 2013

and hypocentral depth are found from the grid search, the seismic moment is determined. For this purpose, the energy of all traces is determined by calculating the sum of squares of all waveform samples. The seismic moment is then calculated as the square root of the ratio of the average energy of data and synthetic trace ($\overline{E}_d$, $\overline{E}_s$):

$$M_0 = \sqrt{\frac{\overline{E}_d}{\overline{E}_s}}. \tag{6}$$

The moment magnitude is calculated after (Kanamori, 1977) by:

$$M_w = \frac{2}{3} \lg M_0 - 10.7. \tag{7}$$

Rupture area A_R and the average displacement $\overline{D}$ are estimated after (Wells and Coppersmith, 1994), who proposed empirical relationships between magnitude and rupture parameters for shallow continental intraplate and interplate earthquakes of magnitudes larger than 4.5:

$$\begin{aligned} \lg A_R &= -2.87(\pm 0.5) + 0.82(\pm 0.08)\, M_w \text{ and} \\ \lg \overline{D} &= -4.45(\pm 1.59) + 0.63(\pm 0.24)\, M_w. \end{aligned} \tag{8}$$

6 Results and discussion

6.1 First event

The grid search for focal parameters was applied in steps of 12° for strike and rake, and in steps of 1° for dip. Various low-frequency bandpass filters between 0.02 and 0.1 Hz were tested to reduce the influence of local crustal structures. The best waveform fits were achieved for a bandpass between 0.03–0.07 Hz. When experimenting with the grid search, matching both body and surface wave phases lead to unsatisfactory waveform fits. Either a good fit of the body waveforms or a good fit of the surface waveforms could be achieved. A satisfactory fit of both would at least have required a 2-D earth model that reflects the complex crustal and lithospheric structure along the wave paths which cross the Hellenides, Dinarides and Eastern Alps. Since surface waves are much more affected by such lithospheric complexity than body waves, we restricted ourselves to matching *P* and *S* wave phases only. Regarding focal depth, high-amplitude surface waves clearly visible in analogue seismograms and time-frequency spectra, testify that the earthquake occurred within the overriding Aegean crust and not in the subducting Hellenic slab at about 120–160 km depth (Brüstle, 2012). As the Moho of the Aegean plate in the central HVA lies at 25–27 km depth (e.g. Papazachos and Nolet, 1997; Bohnhoff et al., 2001), we limited the grid-search to hypocentral depths of less than 50 km. Finally, since three slightly differing locations of the earthquake have been proposed in the literature (Comninakis and Papazachos, 1986; Makropoulos et al., 1989) and (Okal et al., 2009), we performed the grid search for all of them.

The best waveform fit for all three locations (Fig. 9) is obtained for a SW–NE normal fault at a depth of about 25 ± 5 km, with either a small dextral motion on a SE dipping fault plane ($\phi = 36^\circ$, $\delta = 62^\circ/67^\circ$, $\lambda = -96^\circ/-108^\circ$) or a small sinistral motion on a NW dipping fault plane ($\phi = 240^\circ$, $\delta = 22^\circ/25^\circ$, $\lambda = -60^\circ/-72^\circ$). The seismic moment M_0 of the preferred solutions ranges between 4.22–7.02×10^{19} Nm. The mean moment magnitude M_w is 7.1. According to (Wells and Coppersmith, 1994) this corresponds to an average rupture area A_R of about 900 km^2 and an average displacement $\overline{D}$ of about 1.0 m. The preferred solution (Fig. 10) is the dextral SE dipping normal fault mechanism, as all three hypocenter determinations located the earthquake along the northern shoulder of the Santorini–Amorgos graben. This is in agreement with seismic reflection profiles showing a SE dipping normal fault along the northern graben shoulder as well as with neotectonic investigations identifying a NW–SE oriented tensional stress field and a coseismic uplift of the south coast of Amorgos of 0.30 m (Papadopoulos and Pavlides, 1992; Stiros et al., 1994). The preferred solution is also in good agreement with previous focal mechanism determinations of (Shirokova, 1972) and (Okal et al., 2009) and the local stress field obtained from studies of recent seismicity (Bohnhoff et al., 2006; Friederich et al., 2013). (Okal et al., 2009) found a similar focal mechanism, but at hypocentral depths of 46 km. This depth seems to be unlikely, as the Moho has been identified no deeper than 20–27 km in the central volcanic arc of the HSZ (e.g. Makris, 1978; Bohnhoff et al., 2001; Sodoudi et al., 2006, 2013; Tirel et al., 2004; Drakatos et al., 1997; Papazachos and Nolet, 1997; Karagianni et al., 2005; Karagianni and Papazachos, 2007; Endrun et al., 2008). The focal depth of the preferred solution of the present study at about 25 ± 5 km seems to be more realistic and corresponds to the observed recent seismic activity of the graben region (Bohnhoff et al., 2006; Brüstle, 2012).

6.2 Second event

The analogue seismograms as well as their time-frequency spectra exhibit a strong interference of surface wave coda from the first event with body waves from the second event in a time window between 17 min and 22 min after origin time. Surface waves from the second event are apparently missing (Fig. 8). Since the body wave phases of the second event are best recognizable at frequencies above 0.15 Hz, a set of various higher frequency bandpass filters between 0.15 and 0.3 Hz were selected to reduce the influence of the surface waves coda of the previous event. The grid search was then carried out for focal depths down to 163 km to cover slab depths beneath the central HVA. Yet, it did not result in a reliable focal mechanism of the second earthquake because the remaining surface wave coda of the first event prevents a trustworthy matching of the body wave signals.

The grid-search was applied to *P* and *S* waves and, if available, to surface waves. For all three locations (Fig. 11), they result in a minimum misfit for depths larger than 135 km. The minimum misfits of 26.4–65.6 are high compared to the minimum misfit of the first event owing to the overlapping surface wave coda of the first event. Waveform misfits extremely increase at depths of less than 40 km owing to the occurrence of strong surface waves in the synthetic seismograms not observed in the digitized recordings. For the location given by (Comninakis and Papazachos, 1986), Fig. 12 compares the best waveform match within the Aegean plate obtained for a hypocentral depth of 18 km with the best waveform match of the entire grid-search obtained for a hypocentral depth of 159 km. Significant surface wave amplitudes in the synthetic waveforms (red) can be observed for the shallow hypocenter which are absent both in the digitized waveforms (black) and in the synthetic waveforms for the deep hypocenter. The seismic moment M_0 calculated for all three locations varies between 3.1×10^{19} and 6.6×10^{19} Nm while moment magnitude M_w varies between 6.96 and 7.18 (Table 4). The great hypocenter depth points to an intermediate-depth earthquake within the WBZ of the subducting Hellenic slab, which is located at 120–160 km depth beneath the Santorini–Amorgos graben (Knapmeyer, 1999; Papazachos et al., 2000; Meier et al., 2007; Brüstle, 2012). Remarkably, recent studies of receiver function analysis (Sodoudi et al., 2013) and local seismicity (Brüstle, 2012) identified a arc normal deformation zone of the subducting Hellenic slab extending from east of Crete to the region beneath the Santorini–Amorgos graben, that separates a more shallowly dipping western slab segment from a more steeply dipping eastern slab segment. We speculate that the second event may be related to this deformation zone. The only slightly smaller size of the second earthquake compared to the first one is surprising in view of the fact that signals of the second event are barely visible in the historic seismograms. Possible explanations are: (1) At many stations recording needles jumped off the recording papers when the surface waves of the first event arrived, and the second event was not recorded at all. (2) On the remaining analogue seismograms the *P* and *S* wave signals of the second event are often masked by the high-amplitude surface wave signals of the first event and can be only clearly identified in the time-frequency spectrum (Fig. 8). There, at least the *P* wave signals show significant amplitudes. The small amplitudes of the *S* waves may be due to differences in the source mechanisms of the two earthquakes. (3) Large surface wave signals are missing for the second event because of the great depth of the hypocenter.

SED
5, 1901–1940, 2013

7 Conclusions

Refined estimates of hypocentral depth and focal mechanism of the large Amorgos twin earthquakes of 9 July 1956 (03:11 and 03:24 GMT) were obtained from historic seismograms by a grid search based on the matching of historic, digitized waveforms to corresponding synthetic seismograms. In total, 80 historic records of the two earthquakes were collected either at European observatories or taken from the SISMOS database (Michelini et al., 2005). After scanning of the analogue recordings, the TESEO software (Pintore et al., 2005) was used to digitize the seismograms and to correct them for distortions. To obtain instrument responses, information bulletins were searched for relevant parameters. Owing to variable recording quality and incomplete documentation of instrument parameters, 7 recordings proved suitable for subsequent analysis of the first earthquake while 4 records could be used for analyzing the second event. High surface wave amplitudes point to a shallow origin of the first earthquake while missing surface waves suggest a deep hypocenter for the second event. These findings are confirmed by a waveform matching grid search for depth and focal mechanism resulting in a SW–NE striking normal faulting mechanism for the first event at a depth of about 25 ± 5 km. The focal mechanism is consistent with both, the location of the epicenter on the northern flank of the Santorini–Amorgos graben, and a crustal thickness of less than 27 km of the Aegean crust in the central HVA. The seismic moment of the first event is estimated to $4.2–7.02 \times 10^{19}$ Nm corresponding to a mean moment magnitude of 7.1, a mean slip on the fault of about 1 m and a mean rupture area of about 900 km^2. Although the Santorini–Amorgos graben is currently characterized by spatially and temporarily varying clusters of microseismic activity confined to the upper crust that are very likely related to fluid flow and the volcanic activity along the fault zone (Dimitriadis et al., 2005; Bohnhoff et al., 2006; Kolaitis et al., 2007; Dimitriadis et al., 2009; Hensch, 2009; Brüstle, 2012; Newman et al., 2012; Chouliaras et al., 2012; Vallianatos et al., 2013), the first of the Amorgos twin earthquakes remains disquieting evidence for the extreme seismic hazard in this area.

Determination of a meaningful focal mechanism for the second earthquake was impossible because of the strong interference of surface wave coda from the first event with body waves from the seond one. Nevertheless, amplitude ratios of body and surface waves from the second event suggest a source at intermediate depths of at least 135 km. This depth range is in agreement with the observed depths of the WBZ of the subducting Hellenic slab beneath the HVA (Knapmeyer, 1999; Papazachos et al., 2000; Meier et al., 2007; Brüstle, 2012). The seismic moment of the second event was estimated to 3.1–6.6 × 10^{19} Nm corresponding to a mean moment magnitude of 7.08 indicating that both earthquakes were of comparable size.

Acknowledgements. The study was funded by the German Research Foundation (DFG) within the Collaborative Research Centre 526 "Rheology of the Earth – From the Upper Crust to the Subduction Zone". The majority of figures was generated with the Generic Mapping Tools (GMT) by (Wessel and Smith, 1995) and the background topography was generated from the ETOPO1 global relief model of (Amante and Eakins, 2009). We would like to thank Alberto Michelini, Graziano Ferrari and SISMOS Working group for scanning the collected seismogram at the INGV, the introduction into the TESEO software and providing additionally scanned seismograms and bulletins. Also, we would like to thank the following persons for providing analogue seismograms, bulletins and the information, which could be read in any bulletin: Ivo Allegretti (University of Zagreb), Manfred Baer (former member of the Swiss Seismological Service SED), Ioannis Baskoutas (National Observatory Athens NOA), Josep Batllo (University of Lisbon, former member of the Ebre Observatory, Spain), Wolfgang Brüstle (Landeserdbebendienst Baden-Württemberg), Wolfgang Brunk (Wiechert'sche Erdbebenwarte Göttingen e.V.), Andreas Tilgner (Georg-August-University Göttingen), Petra Buchholz (University Leipzig), Torsten Dahm (German Research Centre for Geosciences GFZ, former member of University Hamburg), Martin Hensch (University of Iceland, former member of University Hamburg), Pauline Galea (University of Malta), Klaus-G. Hinzen (University of Cologne), Manfred Joswig (University Stuttgart), Wolfgang Lenhardt (ZentralAnstalt für Meteorologie und Geodynamik, Austria), Nurcan Meral Özel (Kandilli Observatory), Wilfried Steinhoff (Göttingen), Tuncay Taymaz (Istanbul Technical University), Roland Verbeiren (former member of the Royal Observatory of Belgium), Pawel Wiejacz (University of Warzawa) and Rolf Schick (former member of University Stuttgart).

References

Amante, C. and Eakins, B.: ETOPO 1 Arc-Minute Global Relief Model: Procedures, Data Sources and Analysis, NOAA Technical Memorandum NESDIS, NGDC-24, 19 pp., 2009. 1918

Ambraseys, N.: The seismic sea wave of July 1956 in the Greek Archipelago, J. Geophys. Res., 65, 1257–1265, 1960. 1904, 1905, 1929

Ambraseys, N.: Reassessment of earthquakes, 1900–1999, in the Eastern Mediterranean and the Middle East, Geophys. J. Int., 145, 471–485, 2001. 1925

Bohnhoff, M., Markis, J., Papanikolaou, D., and Stavrakakis, G.: Crustal investigations of the Hellenic subduction zone using wide aperture seismic data, Tectonophysics, 343, 239–262, 2001. 1903, 1914, 1915

Bohnhoff, M., Rische, M., Meier, T., Becker, D., Stavrakakis, G., and Harjes, H.-P.: Microseismic activity in the Hellenic Volcanic Arc, Greece, with emphasis on the seismotectonic setting of the Santorini-Amorgos zone, Tectonophysics, 423, 17–33, 2006. 1903, 1904, 1915, 1917

Brüstle, A.: Seismicity of the eastern Hellenic Subduction Zone, Ph. D. thesis, Fakultät für Geowissenschaften, Ruhr-Universität Bochum, 2012. 1903, 1904, 1914, 1915, 1916, 1917, 1918

Charlier, C. and Van Gils, J.: Liste des stations seismologiques mondiales, L'association internationale de seismologie, Observatoire Royal de Belgique, 1953. 1908, 1927

Chouliaras, G., Drakatos, G., Makropoulos, K., and Melis, N. S.: Recent seismicity detection increase in the Santorini volcanic island complex, Nat. Hazards Earth Syst. Sci., 12, 859–866, doi:10.5194/nhess-12-859-2012, 2012. 1904, 1917

Comninakis, P. and Papazachos, B.: A catalogue of earthquakes in Greece and the surrounding area for the period 1901–1985, Univ. Thessaloniki Geophys. Lab. Publ., 1986. 1903, 1905, 1914, 1916, 1925, 1926, 1928, 1931, 1937, 1939, 1940

Dimitriadis, I., Panagiotopoulos, D., Papazachos, C., Hatzidimitrou, P., Karagianni, E., and Kane, I.: Recent seismic activity (1994–2002) of the Santorini volcano using data from local seismological network, Dev. Volcanol., 7, 185–203, 2005. 1904, 1917

Dimitriadis, I., Karagianni, E., Panagiotopoulos, D., Papazachos, C., Hatzdimitriou, P., Bohnhoff, M., Rische, M., and Meier, T.: Seismicity and active tectonics at Coloumbo Reef (Aegean Sea, Greece): monitoring an active volcano at Santorini Volcanic Center using a temporary seismic network, Tectonophysics, 465, 136–149, 2009. 1904, 1917

Dominey-Howes, D.: Sedimentary deposits associated with the July 9th 1956 Aegean Sea Tsunami, Phys. Chem. Earth, 21, 51–55, 1996. 1905

Dominey-Howes, D., Cundy, A., and Croudace, I.: High energy marine flood deposits on Astypalea Island, Greece: possible evidence for the AD 1956 southern Aegean tsunami, Mar. Geol., 163, 303–315, 2000. 1905

Drakatos, G., Karantonis, G., and Stavrakakis, G.: *P* wave crustal tomography of Greece with use of an accurate two-point ray tracer, Ann. Geofis., XL, 25–36, 1997. 1903, 1915

Dziewonski, A., Bloch, S., and Landisman, M.: A technique for the analysis of transient seismic signals, Bull. seism. Soc. Am., 59, 427–444, 1969. 1906, 1909

Endrun, B., Meier, T., Lebedev, S., Bohnhoff, M., and Harjes, H.-P.: *S* velocity structure and radial anisotropy in the Aegean region from surfac wave dispersion, Geophys. J. Int., 174, 593–616, 2008. 1903, 1915

Friederich, W. and Dalkolmo, J.: Complete synthetic seismograms for a spherically symmetric earth by a numerical computation of the Green's function in the frequency domain, Geophys. J. Int., 122, 537–550, 1995. 1911

Friederich, W., Brüstle, A., Küperkoch, L., Meier, T., and Egelados Working Group: Focal mechanisms in the Southern Aegean from temporary seismic networks - implications for the regional stress field and ongoing deformation processes, Solid Earth Discuss., 5, 1721–1770, 2013.

Galanopoulos, A.: Tsunamis observed on the coasts of Greece from antiquity to present time, Ann. Geofis., 13, 369–386, 1960. 1905, 1929

Galanopoulos, A.: The damaging shocks and earthquake potential of Greece, Ann. Geol. Pays Hellen., 30, 648–724, 1982. 1905, 1925

Galizin, F. B.: Vorlesung über Seismometrie, Verlag B. G. Teubner, Leizig und Berlin, 1914. 1909

Gerecke, F.: Seismische Registrierungen in Jena, 1. Januar 1948 bis 31. Dezember 1949, Deutsche Akademie der Wissenschaften zu Berlin, Veröffentlichungen des Zentralinstitutes für Erdbebenforschung in Jena, 54, Akademie Verlag Berlin, Berlin, 1950. 1927

Gerecke, G. and Güth, D.: Seismische Registrierungen der Nebenstation von Jena, Potsdam, Halle, Plauen und Sonneberg 1957, Deutsche Akademie der Wissenschaften zu Berlin, Veröffentlichungen des Institutes für Bodendynamik und Erdbebenforschung in Jena, 64, Akademie Verlag Berlin, Berlin, 1961. 1932

Hensch, M.: On the interrelation of fluid-induced seismicity and crustal deformation at the Coloumbo Submarine Volcano (Aegean Sea, Greece), Ph. D. thesis, Institut für Geophysik, Universität Hamburg, Hamburg, 2009. 1904, 1917

Hiller, W.: Seismischer Bericht des Württembergischen Erdbebendienstes, Veröffentlichungen des Landeserdbebendienstes Baden-Württemberg, Stuttgart, 1951. 1932

Hiller, W. and Schneider, G.: Seismischer Jahresbericht 1960, Veröffentlichungen des Landeserdbebendienstes Baden-Württemberg, Stuttgart, 1962. 1927

Jensen, H.: Bulletin of the seismological station København, Geodætisk institut Proviantgården, Copenhagen, Denmark, 66, 1957. 1927

Kanamori, H.: The energy release in great earthquakes, J. Geophys. Res., 82, 2981–2987, 1977. 1913

Karagianni, E. and Papazachos, C.: Shear velocity structure in the Aegean region obtained by joint inversion of Rayleigh and Love waves, in: The Geodynamics of the Aegean and Anatolia, edited by: Taymaz, T., Yilmaz, Y., and Dilek, Y., Geological Society, London, Special Publications, 291, 159–181, 2007. 1903, 1915

Karagianni, E., Panagiotopoulos, D., Panza, G., Suhadolc, P., Papazachos, C., Papazachos, B., Kiratzi, A., Hatzfeld, D., Makropoulos, K., Priestley, K., and Vuan, A.: Rayleigh wave group velocity tomography in the Aegean area, Tectonophysics, 358, 187–209, 2002. 1903

Karagianni, E., Papazachos, C., Panagiotopoulos, D., Suhadolc, P., and Vuan, A. Panza, G.: Shear velocity structure in the Aegean area obtained by inversion of Rayleigh waves, Geophys. J. Int., 160, 127–143, 2005. 1903, 1915

Kennett, B., Engdahl, E., and Buland, R.: Constraints on seismic velocities in the Earth from traveltimes, Geophys. J. Int., 122, 108–124, 1995. 1911

Knapmeyer, M.: Geometry of the Aegean Benioff zones, Ann. Geofis., 42, 27–38, 1999. 1904, 1916, 1918

Kolaitis, A., Papadimiriou, P., Kassaras, I., and Makropoulos, K.: Seismic observations with broadband instruments at Santorini volcano, Bulletin of the Geological Society of Greece, Proceedings of the 11th international Congress, Athens, XXXX, 1150–1161, 2007. 1904, 1917

Makris, J.: The crust and upper mantle of the Aegean region from deep seismic soundings, Tectonophysics, 46, 269–284, 1978. 1903, 1915

Makropoulos, K., Drakopoulos, J., and Latousakis, J.: A revised and extended earthquake catalogue for Greece since 1900, Geophys. J. Int., 98, 391–394, 1989. 1903, 1905, 1914, 1925, 1928, 1937, 1939

McKenzie, D.: Plate Tectonics of the Mediterranean Region, Nature, 226, 239–243, 1970. 1903

McKenzie, D.: Active tectonics of the Mediterranean region, Geophys. J. Roy. Astr. S., 30, 109–185, 1972. 1903

Meier, T., Dietrich, K., Stöckert, B., and Harjes, H.-P.: One-dimensional models of shear-wave velocity for eastern Mediterranean obtained from the inversion of Rayleigh wave phase velocities and tectonic implications, Geophys. J. Int., 156, 45–58, 2004. 1910

Meier, T., Becker, D., Endrun, B., Rische, M., Bohnhoff, M., Stöckert, B., and Harjes, H.-P.: A model for the Hellenic subduction zone in the area of Crete based on seismological investigations, Geological Society, London, Special Publications, 291, 183–199, 2007. 1904, 1916, 1918

Michelini, A., De Simoni, B., Amato, A., and Boschi, E.: Collecting, Digitizing, and Distributing Historical Seismological Data, EOS, Trans. Am. Geophys. Un., 86, 261–266, 2005. 1906, 1917

Newman, A., Stiros, S., Feng, L., Psimoulis, P., Moschas, F., Saltogianni, V., Jiang, Y., Papazachos, C., Panagiotopoulos, F., Karagianni, E., and Vamvakaris, D.: Recent geodetic unrest at Santorini Caldera, Greece, Geophys. J. Int., 39, L063091, doi:10.1029/2012GL051286, 2012. 1904, 1917

Okal, E., Synolakis, C., Uslu, B., Kalligeris, N., and Voukouvalas, E.: The 1956 earthquake and tsunami in Amorgos, Greece, Geophys. J. Int., 178, 1533–1554, 2009. 1903, 1905, 1906, 1914, 1915, 1925, 1928, 1937, 1939

Papadopoulos, G. and Pavlides, S.: The large 1956 earthquake in the South Aegean: Macroseismic field configuration, faulting, and neotectonics of Amorgos Island, Earth Planet. Sci. Lett., 113, 383–396, 1992. 1904, 1914, 1929

Papazachos, B.: A lithospheric model to interpret focal properties of intermediate and shallow shocks in Central Greece, Pageoph., 117, 655–666, 1977. 1903

Papazachos, B. and Delibasis, N.: Tectonic stress field and seismic faulting in the area of Greece, Tectonophysics, 7, 231–255, 1969. 1905

Papazachos, B. and Nolet, G.: P and S deep velocity structure of the Hellenic area obtained by robust nonlinear inversion of travel times, J. Geophys. Res., 102, 8349–8367, 1997. 1903, 1914, 1915

SED
5, 1901–1940, 2013

Papazachos, B., Karakostas, V., Papazachos, C., and Scoridilis, E.: The geometry of the Wadati-Benioff zone and lithospheric kinematics in the Hellenic arc, Tectonophysics, 319, 275–300, 2000. 1904, 1916, 1918

Perissoratis, C. and Papadopoulos, G.: Sediment instability and slumping in the southern Aegean Sea and the case history of the 1956 tsunami, Mar. Geol., 161, 287–305, 1999. 1904

Pintore, S., Quintiliani, M., and Franceschi, D.: Teseo: a vectoriser of historical seismograms, Comput. Geosci., 31, 1277–1285, 2005. 1906, 1917

Reilinger, R., McClusky, S., Vernant, P., Lawrence, S., Ergintav, S., Cakmak, R., Ozener, H., Kadirov, F., Guliev, I., Stepanyan, R., Nadyriya, M., Hahubia, G., Mahmoud, S., Sakr, K., Ar-Rajehi, A., Paradissis, D., Al-Aydrus, A., Prilepin, M., Guseva, T., Evren, E., Dmitrotsa, A. Filikov, S., Gomez, F., Al-Ghazzi, R., and Karam, G.: GPS constraints on continental deformation in the African-Arabian-Eurasia continental collision zone and implications for the dynamics of plate interactions, J. Geophys., 111, B05411, 1–26, 2006. 1903

Ritsema, A.: Earthquake mechanisms of the Balcan region, R. Neth. Meteorol. Inst., Sci. Rep., 74, 36, 1974. 1905

Schick, R. and Schneider, G.: Physik des Erdkörpers, Ferdinand Enke Verlag Stuttgart, 1973. 1909

Shirokova, E.: Sress pattern and probable motion in the earthquake foci of the Asia-Mediterranean seismic belt, in: Elastic Strain Field of the Earth and Mechanisms of Earthquake Sources, edited by: Balakina, L. M., Vvedenskaya, A. V. , Golubeva, N. V., Misharina, L. A., Shirokova, E. I., Nauka, Moscow, 1972. 1905, 1915

Sodoudi, F., Kind, R., Hatzfeld, D. Priestley, K., Hanka, W., Wylegalla, K., Stavrakakis, G., Vafidis, A., Harjes, H.-P., and Bohnhoff, M.: Lithospheric structure of the Aegean obtained from *P* and *S* receiver functions, J. Geophys. Res., 111, B12307, doi:10.1029/2005JB003932, 2006. 1903, 1915

Sodoudi, F., Bruestle, A., Meier, T., Kind, R., Friederich, W., and EGELADOS working group: New constraints on the geometry of the subducting African plate and the overriding Aegean plate obtained from P receiver functions and seismicity, Solid Earth Discuss., 5, 427–461, doi:10.5194/sed-5-427-2013, 2013. 1903, 1915, 1916

Stiros, S., Maraou, L., and Arnold, M.: Quarternary uplift and tilting of Amorgos Island (southern Aegean) and the 1956 earthquake, Earth Planet. Sci. Lett., 128, 65–76, 1994. 1904, 1905, 1914

SED
5, 1901–1940, 2013

Tirel, C., Gueydan, F., Tiberi, C., and Brun, J.-P.: Aegean crustal thickness inferred from gravity inversion, geodynamical implications, Earth Planet. Sci. Lett., 228, 267–280, 2004. 1903, 1915

Vallianatos, F., Michas, G., Papadakis, G., and Tzanis, A.: Evidence of non-extensivity in the seismicity observed during the 2011–2012 unrest at the Santorini volcanic complex, Greece, Nat. Hazards Earth Syst. Sci., 13, 177–185, doi:10.5194/nhess-13-177-2013, 2013. 1904, 1917

Wells, D. and Coppersmith, K.: New Empirical Relationships among Magnitude, Rupture Length, Rupture Width, Rupture Area and Surface Displacement, Bull. seism. Soc. Am., 84, 974–1002, 1994. 1913, 1914

Wessel, P. and Smith, W.: New version of the Generic Mapping Tool released, EOS, Trans. Am. Geophys. Un., 76, 329, 1995. 1918

Wielandt, E.: Seismographen, in: Wechselwirkungen, Jahrbuch aus Lehre und Forschung der Universität Stuttgart, available at: http://elib.uni-stuttgart.de/opus/volltexte/1999/488 (last access: 5 November 2013) 1996. 1912

SED

5, 1901–1940, 2013

Focal mechanism and depth of the 1956 Amorgos twin earthquakes

A. Brüstle et al.

Table 1. Hypocenter parameters of the two earthquakes on 9 July 1956 from previous studies indicate a large uncertainty of hypocentral depth.

Author	Event time (GMT)	Location	Depth (km)	Magnitude
(Galanopoulos, 1982)		36.7° N, 25.9° E	10 (+3)	7.5 M_S
		36.6° N, 25.9° E	40 (+30)	6.75 M_S
(Comninakis and Papazachos, 1986)	03:11:40	36.7° N, 25.8° E	< 70	7.5 M_S
	03:24:03	36.6° N, 25.7° E	< 70	6.9 M_S
(Makropoulos et al., 1989)	03:11:43.7	36.64° N, 25.92° E	15 (+10)	7.4 M_S
	03:24:16.5	36.45° N, 25.51° E	95 (+15)	7.2 M_S
(Ambraseys, 2001)	03:11	36.72° N, 25.80° E	15	7.18 M_S
	03:24	36.65° N, 25.70° E	30	6.00 M_S
(Okal et al., 2009)	03:11:45	36.72° N, 25.76° E	45	$3.9 \cdot 10^{27*}$
	03:24:07	36.39° N, 25.78° E	–	–

* dyn cm M_0.

SED
5, 1901–1940, 2013

Focal mechanism and depth of the 1956 Amorgos twin earthquakes

A. Brüstle et al.

Table 2. Station coordinates associated with analogue seismograms used in the present study. Distances are given relative to the hypocenter location of the first earthquake after (Comninakis and Papazachos, 1986).

Station	Lat (N)	Lon (E)	Elevation (m)	Epicenter dist. (km)	Epicenter dist. (°)
STU	48.7719	9.1950	360.0	1907.3	17.183
JEN	50.9350	11.5830	195.0	1949.1	17.559
GTT	51.5464	9.9642	272.0	2073.7	18.682
COP	55.6853	12.4325	13.0	2337.2	21.056

SED
5, 1901–1940, 2013

Table 3. Instrument parameters that seismograph systems of the recorded analogue seismograms used in the present study. Component polarity in writing direction: left is up (+), right is down (–).

Station	Seismometer	Comp.	Mass k [kg]	Eigenperiod To [sec]	Amplification V	Damping ϵ:1	Comp. polarity
STU[1,2,6]	Mainka	*N*	450	10	120	4.5	*N*+/*S*–
STU[1,2,6]	Mainka	*E*	450	10	120	4.5	*E*+/*W*–
JEN[3,6]	Wiechert	*Z*	1300	2.5	250	2.4	*U*+/*D*–
GTT[4]	Wiechert	*Z*	1300	5	182	3.3	*U*–/*D*+
GTT[4]	Wiechert	*N*	1200	11	130	3.8	*S*+/*N*–
GTT[4]	Wiechert	*E*	1200	10.8	125	2.7	*W*+/*E*–
COP[5,6]	Wiechert	*N*	1000	8.5	210	4.0	*S*+/*N*–
COP[5,6]	Wiechert	*E*	1000	8.5	210	4.0	*W*+/*E*–

[1] (Hiller and Schneider, 1962), [2] R. Schick, personal communication, 2006, [3] (Gerecke, 1950), [4] written on the seismograms, [5] (Jensen, 1957), [6] (Charlier and Van Gils, 1953)

SED

5, 1901–1940, 2013

Focal mechanism and depth of the 1956 Amorgos twin earthquakes

A. Brüstle et al.

Table 4. Total waveform misfit, seismic moment, moment magnitude and focal depth of the two earthquakes on 9 July 1956.

Author	Misfit χ^2	Seismic moment M_0 (Nm)	Moment magnitude M_w	Depth (km)
1st earthquake				
(Comninakis and Papazachos, 1986)	1.22	4.44×10^{19}	7.06	25
(Makropoulos et al., 1989)	1.47	4.22×10^{19}	7.05	25
(Okal et al., 2009)	1.07	7.02×10^{19}	7.19	21
2nd earthquake				
(Comninakis and Papazachos, 1986)	26.34	5.3×10^{19}	7.11	159.54
(Makropoulos et al., 1989)	46.51	3.1×10^{19}	6.96	162.27
(Okal et al., 2009)	65.61	6.6×10^{19}	7.18	162.27

SED
5, 1901–1940, 2013

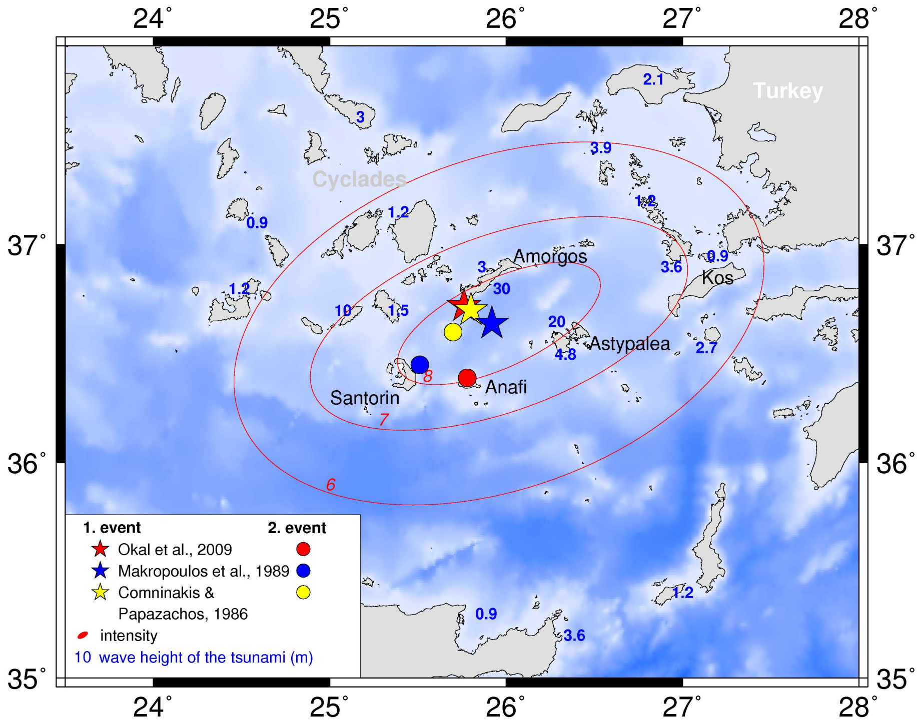

Fig. 1. Map of locations of the two earthquakes on 9 July 1956 at 03:11 and 03.24 UTC investigated in this study. Intensities (red numbers and ellipses) were taken from (Papadopoulos and Pavlides, 1992) and tsunami heights (blue numbers) from (Ambraseys, 1960) and (Galanopoulos, 1960).

SED
5, 1901–1940, 2013

Fig. 2. Fault plane solutions for the first earthquake from previous studies.

SED
5, 1901–1940, 2013

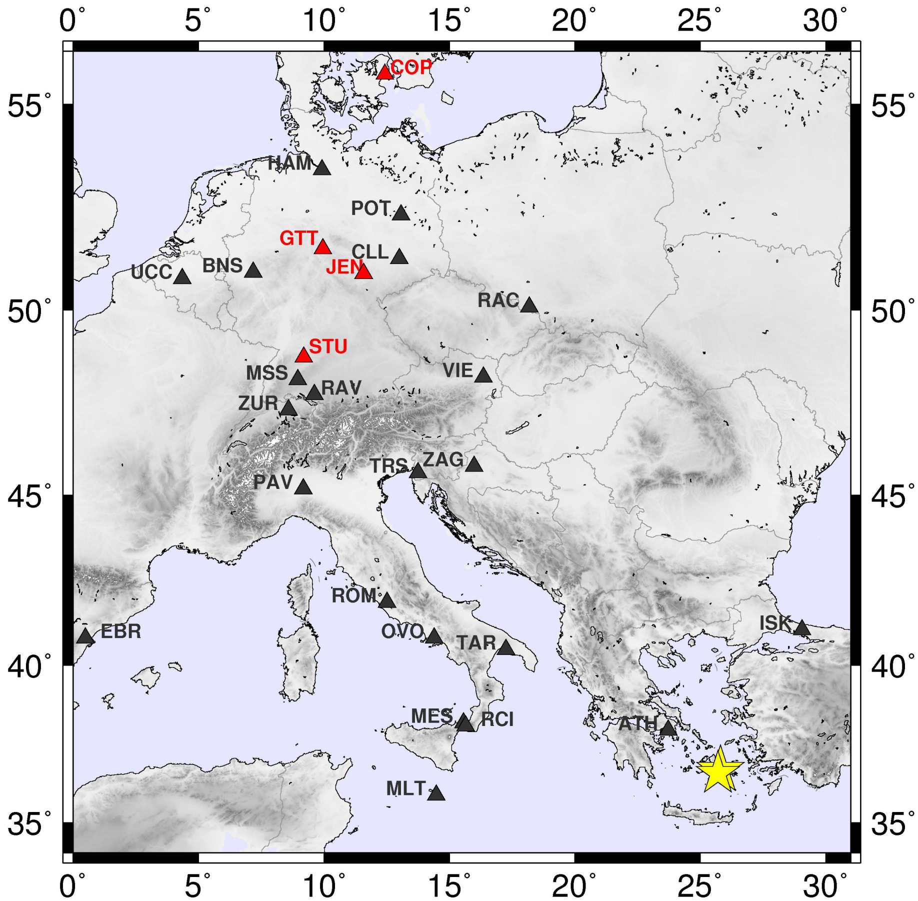

Fig. 3. Station map for the more than 80 collected analogue seismograms from 29 European stations. 7 components of the stations STU, GTT and COP for the first and 4 components of the stations JEN, GTT and COP for the second earthquake (yellow stars, Comninakis and Papazachos, 1986) were suitable for the present study.

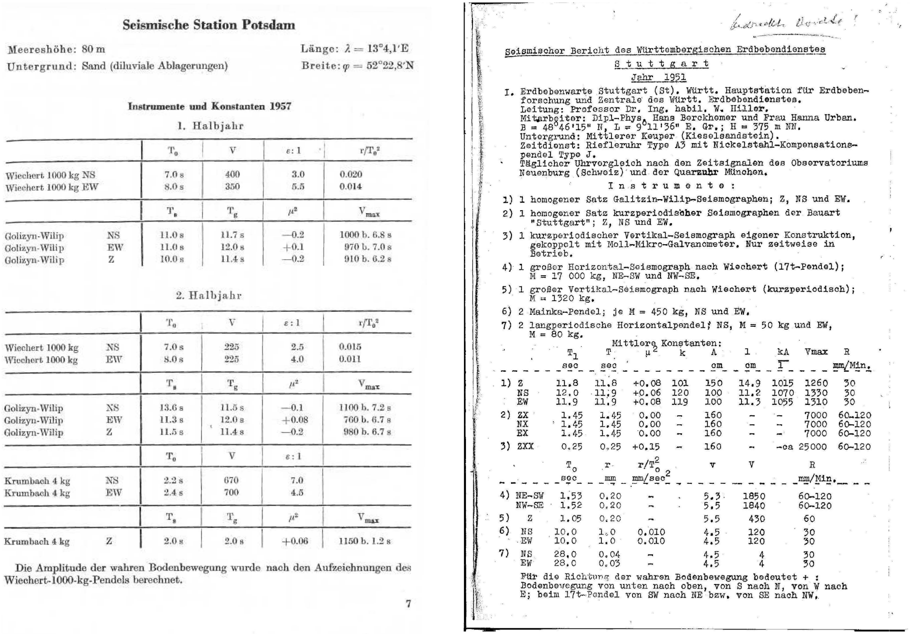

Seismische Station Potsdam

Meereshöhe: 80 m — Länge: $\lambda = 13°4{,}1'E$

Untergrund: Sand (diluviale Ablagerungen) — Breite: $\varphi = 52°22{,}8'N$

Instrumente und Konstanten 1957

1. Halbjahr

		T_0	V	$\varepsilon:1$	r/T_0^2
Wiechert 1000 kg	NS	7.0 s	400	3.0	0.020
Wiechert 1000 kg	EW	8.0 s	350	5.5	0.014
		T_s	T_g	μ^2	V_{max}
Golizyn-Wilip	NS	11.0 s	11.7 s	—0.2	1000 b. 6.8 s
Golizyn-Wilip	EW	11.0 s	12.0 s	+0.1	970 b. 7.0 s
Golizyn-Wilip	Z	10.0 s	11.4 s	—0.2	910 b. 6.2 s

2. Halbjahr

		T_0	V	$\varepsilon:1$	r/T_0^2
Wiechert 1000 kg	NS	7.0 s	225	2.5	0.015
Wiechert 1000 kg	EW	8.0 s	225	4.0	0.011
		T_s	T_g	μ^2	V_{max}
Golizyn-Wilip	NS	13.6 s	11.5 s	—0.1	1100 b. 7.2 s
Golizyn-Wilip	EW	11.3 s	12.0 s	+0.08	760 b. 6.7 s
Golizyn-Wilip	Z	11.5 s	11.4 s	—0.2	980 b. 6.7 s
		T_0	V	$\varepsilon:1$	
Krumbach 4 kg	NS	2.2 s	670	7.0	
Krumbach 4 kg	EW	2.4 s	700	4.5	
		T_s	T_g	μ^2	V_{max}
Krumbach 4 kg	Z	2.0 s	2.0 s	+0.06	1150 b. 1.2 s

Die Amplitude der wahren Bodenbewegung wurde nach den Aufzeichnungen des Wiechert-1000-kg-Pendels berechnet.

7

Seismischer Bericht des Württembergischen Erdbebendienstes

Stuttgart

Jahr 1951

I. Erdbebenwarte Stuttgart (St). Württ. Hauptstation für Erdbebenforschung und Zentrale des Württ. Erdbebendienstes.
Leitung: Professor Dr. Ing. habil. W. Hiller.
Mitarbeiter: Dipl-Phys. Hans Berckhemer und Frau Hanna Urban.
B = 48°46'15" N, L = 9°11'36" E. Gr.; H = 375 m NN.
Untergrund: Mittlerer Keuper (Kieselsandstein).
Zeitdienst: Riefleruhr Type A3 mit Nickelstahl-Kompensationspendel Type J.
Täglicher Uhrvergleich nach den Zeitsignalen des Observatoriums Neuenburg (Schweiz) und der Quarzuhr München.

Instrumente:

1) 1 homogener Satz Galitzin-Wilip-Seismographen; Z, NS und EW.
2) 1 homogener Satz kurzperiodischer Seismographen der Bauart "Stuttgart"; Z, NS und EW.
3) 1 kurzperiodischer Vertikal-Seismograph eigener Konstruktion, gekoppelt mit Moll-Mikro-Galvanometer. Nur zeitweise in Betrieb.
4) 1 großer Horizontal-Seismograph nach Wiechert (17t-Pendel); M = 17 000 kg, NE-SW und NW-SE.
5) 1 großer Vertikal-Seismograph nach Wiechert (kurzperiodisch); M = 1320 kg.
6) 2 Mainka-Pendel; je M = 450 kg, NS und EW.
7) 2 langperiodische Horizontalpendel; NS, M = 50 kg und EW, M = 80 kg.

Mittlere Konstanten:

		T_1 sec	T sec	μ^2	k	A cm	l cm	$\frac{kA}{l}$	Vmax	R mm/Min.
1)	Z	11.8	11.8	+0.08	101	150	14.9	1015	1260	30
	NS	12.0	11.9	+0.06	120	100	11.2	1070	1330	30
	EW	11.9	11.9	+0.08	119	100	11.3	1055	1310	30
2)	ZX	1.45	1.45	0.00	–	160	–	–	7000	60-120
	NX	1.45	1.45	0.00	–	160	–	–	7000	60-120
	EX	1.45	1.45	0.00	–	160	–	–	7000	60-120
3)	ZXX	0.25	0.25	+0.15	–	160	–	–ca	25000	60-120

		T_0 sec	r mm	r/T_0^2 mm/sec^2	v	V	R mm/Min.
4)	NE-SW	1.53	0.20	–	5.3	1850	60-120
	NW-SE	1.52	0.20	–	5.5	1840	60-120
5)	Z	1.05	0.20	–	5.5	430	60
6)	NS	10.0	1.0	0.010	4.5	120	30
	EW	10.0	1.0	0.010	4.5	120	30
7)	NS	28.0	0.04	–	4.5	4	30
	EW	28.0	0.03	–	4.5	4	30

Für die Richtung der wahren Bodenbewegung bedeutet + : Bodenbewegung von unten nach oben, von S nach N, von W nach E; beim 17t-Pendel von SW nach NE bzw. von SE nach NW.

Fig. 4. Extract of the Bulletin of the stations Potsdam (POT), Halle, Plauen and Sonneberg (left). In 1957, instrument parameters were changed twice at the station POT (Gerecke and Güth, 1961). Extract of the Bulletin "Seismischer Bericht des Württembergischen Erdbebendienstes" of 1951 (right). At the station STU 7 seismograph systems were installed recording on smoked and photo-optical paper (Hiller, 1951).

SED
5, 1901–1940, 2013

Focal mechanism and depth of the 1956 Amorgos twin earthquakes

A. Brüstle et al.

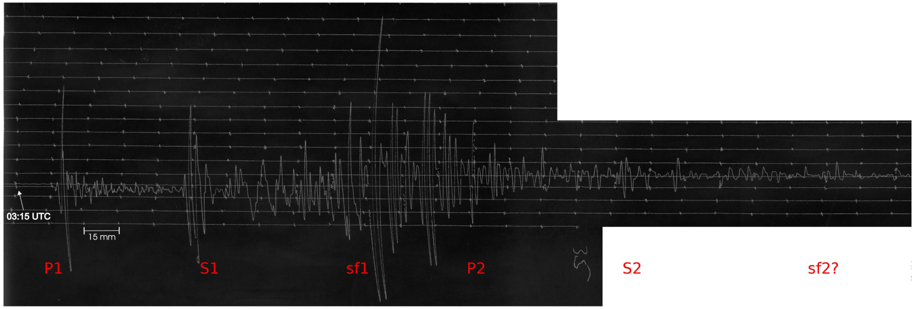

Fig. 5. Scanned analogue seismogram from the original smoked paper of the first earthquake on 9 July 1956. The *Z* component of the 1300 kg-Wiechert seismograph at the station GTT is at about 2073 km distance from the epicenter. Body waves (*P*1, *S*1) and surface waves (sf1) of the first earthquake are recorded in high quality. The recording is clipped at the largest amplitude of the recording and following signals are recorded with an offset of 5–10 mm. Theoretical calculated phase arrivals (P2, S2, sf2?) show that the waveform of the second earthquake is hidden by the surface waves of the first earthquake. Component polarity is inverse to the real ground motion (UP on the seismogram recording is DOWN for real ground motion).

SED
5, 1901–1940, 2013

Focal mechanism and depth of the 1956 Amorgos twin earthquakes

A. Brüstle et al.

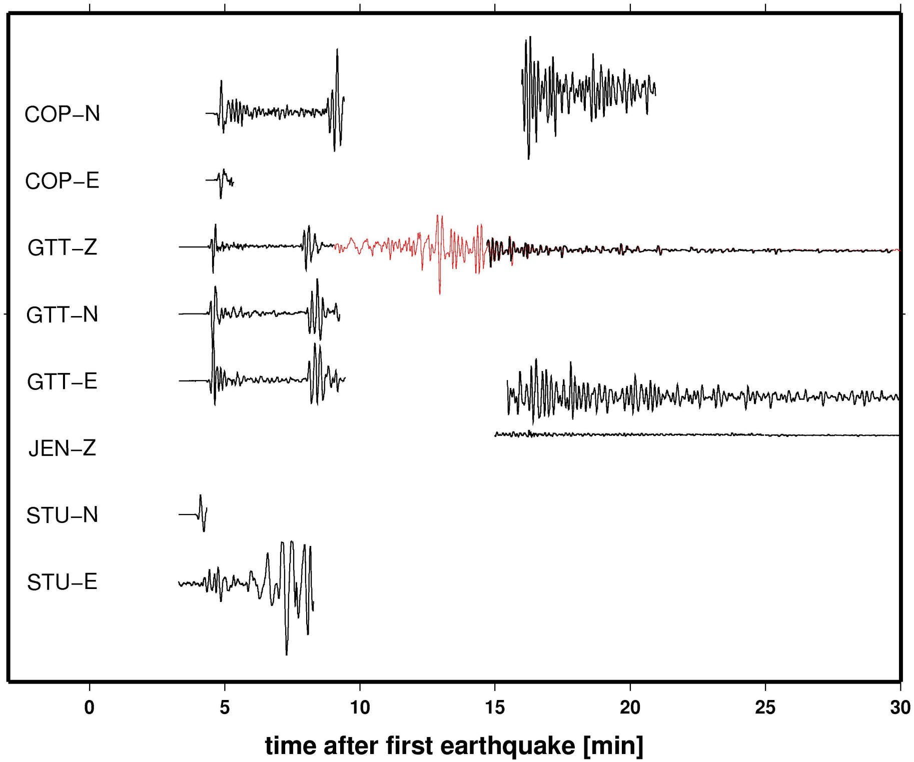

Fig. 6. Usable waveforms (black) of the first earthquake show *P* waves arriving 4–6 min and *S* waves 6–8 min after origin time, while body waves of the second earthquake (15–20 min) are hidden in the surface wave coda of the preceding earthquake. The continously digitized waveform of the *Z* component at station GTT (red) is clipped during the recording of the surface waves of the first event at 13 min (negative offset).

SED
5, 1901–1940, 2013

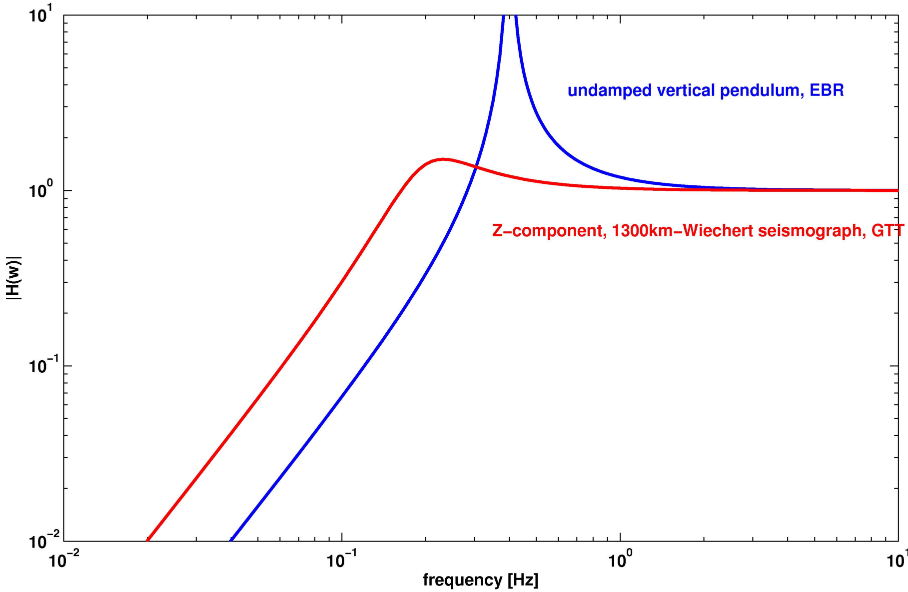

Fig. 7. Frequency-dependent normalized transfer functions of a nearly optimally damped (station GTT, red) and an undamped (station EBR, blue) mechanical seismometer. The transfer function of the Z component of the 1300 kg-Wiechert seismograph shows a constant plateau for frequencies greater than 0.2 Hz. In contrast, a resonance from 0.18 to 1.26 Hz of the undamped vertical pendulum disturbs the recordings significantly.

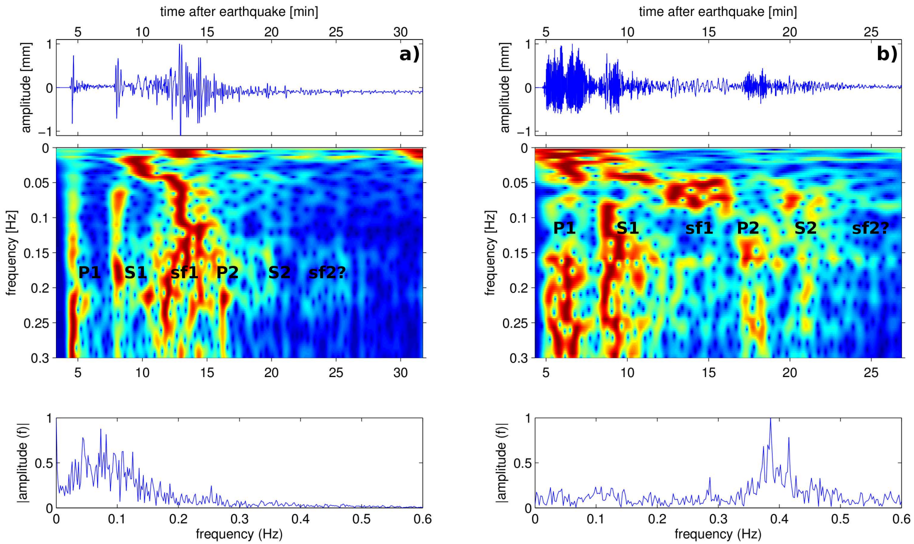

Fig. 8. Digitized waveform (upper part), time-frequency spectra (middle part) and frequency-amplitude spectra (lower part) of digitized unfiltered waveforms of **(a)** the *Z* component of a 1300 kg-Wiechert seismograph at station GTT and **(b)** an undamped vertical pendulum at station EBR. Both digitized seismograms clearly show *P* and *S* phases and dispersed surface waves from the first earthquake, whereas the body phase arrivals from the second earthquake can only be identified in the time-frequency spectrogram. The absence of surface waves in both recordings from the second earthquake indicates a large hypocentral depth.

SED
5, 1901–1940, 2013

Focal mechanism and depth of the 1956 Amorgos twin earthquakes

A. Brüstle et al.

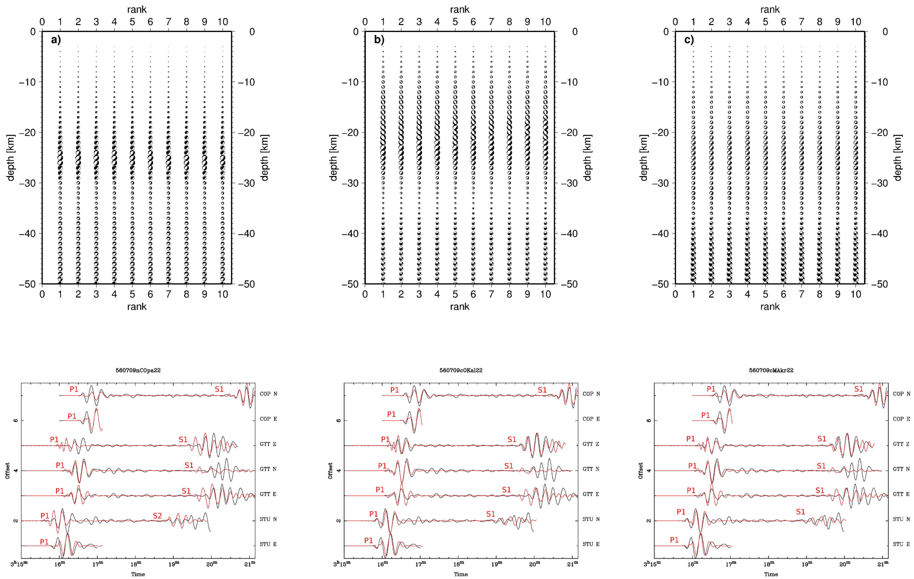

Fig. 9. Upper part: best 10 focal solutions per depth obtained from matching digitized to synthetic waveforms for the first earthquake and hypocenter locations of **(a)** (Comninakis and Papazachos, 1986), **(b)** (Okal et al., 2009) and **(c)** (Makropoulos et al., 1989). The size of the beach balls scales inversely with misfit value. All focal solutions indicate SW–NE striking normal faulting at hypocentral depth of 25 ± 5 km. Lower part: the corresponding digitized (black) and synthetic (red) waveforms at 25 km hypocentral depth are bandpass filtered from 0.03–0.07 Hz and the mistfit values χ^2 range from 1.078 to 1.467.

SED
5, 1901–1940, 2013

strike=36°, dip=62°, rake=−96°

strike=36°, dip=67°, rake=−108°

Fig. 10. Preferred fault plane solutions for the first earthquake.

SED

5, 1901–1940, 2013

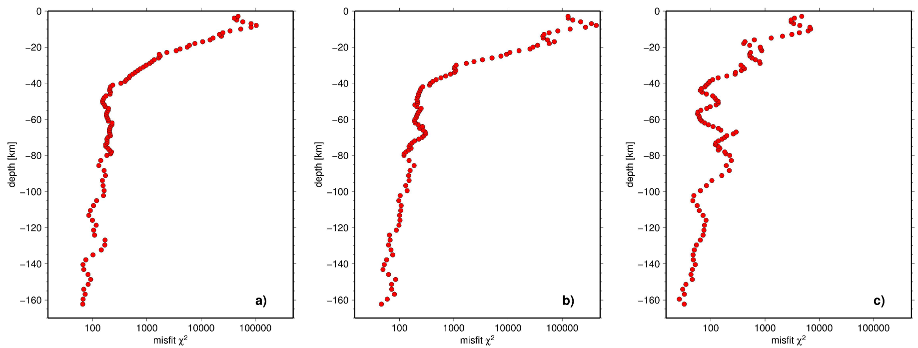

Fig. 11. Minimum waveform misfit vs. depth for the locations of **(a)** (Okal et al., 2009), **(b)** (Makropoulos et al., 1989) and **(c)** (Comninakis and Papazachos, 1986).

SED
5, 1901–1940, 2013

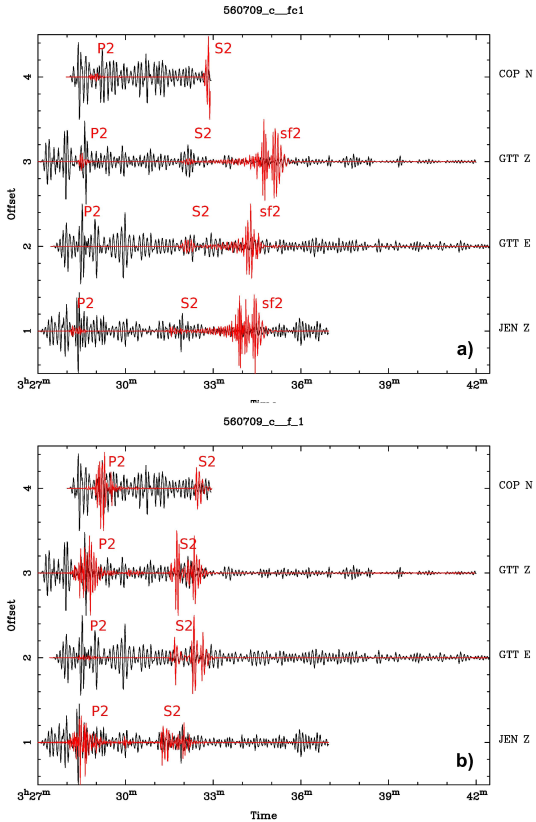

Fig. 12. Comparison of bandpass filtered (0.15–0.3 Hz) digitized waveforms (black) and synthetic seismograms (red) calculated for the best-fitting focal solution at a depth of **(a)** 18 km and the best-fitting focal soluction of the entire grid-search down to 163 km at a depth of **(b)** 159 km. Epicentral location of (Comninakis and Papazachos, 1986) was assumed. Note strong surface waves of the synthetic seismograms for shallow source at 33–35 s not observed in the digitized data, indicating a subcrustal origin of the second earthquake.

SED
5, 1901–1940, 2013